Computational Studies Suggest Promiscuous Candida antarctica Lipase B as an Environmentally Friendly Alternative for the Production of Epoxides

Miquel A. Galmés, Katarzyna Świderek, Vicent Moliner**

Institute of Advanced Materials (INAM), Universitat Jaume I, 12071 Castellón, Spain

Corresponding authors:

swiderek@uji.es

moliner@uji.es

ABSTRACT

Environmentally friendly processes are nowadays a trending topic to get highly desired chemical compounds and, in this sense, the use of enzyme catalyzed routes is becoming a promising alternative to traditional synthetic methods. In the present paper a hybrid QM/MM computational study on the epoxidation of alkenes catalyzed by the Ser105Ala variant of the promiscuous *Candida antarctica* Lipase B (CALB) is presented, in an attempt to search for alternative paths to get useful intermediates in industry. The catalyzed reaction, described at the atomistic level with a model of the full solvated in a box of water molecules, is compared with the alternative epoxidation of alkenes by peroxy-acids in chloroform. Free energy profiles obtained at DFT/MM level show how Ser105Ala CALB is capable of epoxide short alkenes in a two steps process with free energy barriers, in agreement with available experimental data, that are significantly lower than that of the single-step reaction in solution. The possible (R)- enantioselectivity dictated by the binding step, explored by means of alchemical QM/MM FEP methods, and the preference for the (S)-enantiomer derived from the free energy landscape of the chemical steps, would cancel out thus predicting the lack of enantioselectivity experimentally observed. In general, our results provide general information on the molecular mechanism employed by a highly promiscuous enzyme, with potential applications in biotechnology.

Graphic for Table of Contents (TOC)/Abstract Art.

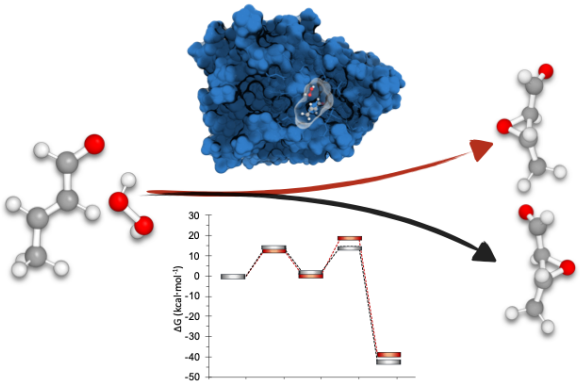

INTRODUCTION

The interest in the study of mechanisms of promiscuous enzymes has recently increased in the field of biomolecular transformations.[1–6] Deep knowledge on how these mechanisms work at a molecular level can lead to new tools that permit obtaining highly desirable chemical compounds, with improved yields, ecological procedures and in a wide variety of conditions. In a world that demands greener sources of products and where the ecological consciousness is an urgent topic, enzymatic approaches are preferred over chemical synthesis.[7]

Enzymes are known for their ability to catalyze chemical reactions in aqueous solution with high efficiency and selectivity under mild conditions of temperature or pressure, resulting in few unwanted side-products. This converts the enzymatic synthesis in an extremely useful tool to obtain chemical compounds in a more ecologically responsible way than the traditional methods that are usually potentially harmful to the environment. An example of these classical chemical methods can be found in the epoxidation of alkenes employing peroxy-acids, known as Prilezhaev reaction.[8] Firstly described at the beginning of the 20th century, this epoxidation of alkenes using peroxy-acids proceeds through a single concerted step where it is believed that the peroxide is positioned perpendicular to the plane of the alkene in the transition state. This mechanism is also known as the *butterfly* mechanism as coined in the middle of 20th century by Paul D. Bartlett,[9] later confirmed by Azman and co-workers,[10] and by Kendall and co-workers[11] based on computational studies and kinetic isotope effects determinations.

Epoxides are very useful and important chemicals in the industry. They are used in the fabrication of surfactants and detergents, insecticides, resins and aerosols, or as stabilizers in coatings and plastic industry.[12,13] The main drawback in the peroxidation of alkenes is the non-environmentally green character of their synthesis. For instance, the use of stoichiometric

amounts of peroxy-acids for epoxidation of alkenes,[14] metal-based catalyzed reactions,[15] epoxidations using hydrogen peroxide in ionic liquids or deep eutectic solvents[16] and manganese salts[17] are some of the established methods for the chemical synthesis of peroxides. For this reason, chemoenzymatic synthesis of epoxides is gaining attention in the industry for its greener character. The use of enzymes would permit to reduce the number of oxidants needed for the epoxidations of alkenes, due to its highly efficient and selective behavior. In this regard, haloperoxidases and monooxygenases are enzymes that catalyze the epoxidation of alkenes but their use in industry is very limited due to their low versatility in cheap and efficient conditions.[18,19]

Over the years many lipases have been reported to be capable of performing secondary reactions,[1,2] but the understanding of the molecular mechanism that governs this promiscuity is still poor. Lipases are very robust enzymes that can work in a wide range of conditions. Moreover, its resistance to organic solvents and oxidants makes this family of enzymes an attractive biocatalyst for the industry. Additionally, it has been described that many lipases can use hydrogen peroxide as oxidant, which is preferred due to its low environmental impact.[16,20,21]

One of the best characterized enzymes in this field is *Candida antarctica* Lipase B (CALB). CALB is widely used in industry, and has served as a model to study enzyme promiscuity, either by experimental and theoretical approaches.[20,22–25] CALB has been demonstrated to be able to perform a wide variety of promiscuous reactions, such as synthesis of esters and amides, transacylation of alcohols,[26] epoxidation reactions,[20] aldol additions and Michael type additions,[2,27] among many others.[2,28] It has been proposed that this serine hydrolase performs its activity due to the presence of a catalytic triad Ser/His/Asp in the active site, as well as an oxyanion hole formed by a Thr and a Gln, that stabilizes the negative charge accumulating on the

carbonyl oxygen atom of the substrate in different states along the reaction. The hydrolytic character of CALB is achieved by the catalytic Ser105. CALB has been previously reported to display epoxidation activity on short alkenes[20] but its hydrolytic activity also permits the ring-opening of epoxides.[23] For this reason the mutation of Ser105 to Ala105 has demonstrated to maximize its catalytic activity in the epoxidation reaction.[20,21]

Besides the direct epoxidation of alkenes, CALB has also been used to produce epoxides from the generation of peroxy-acids.[29] This strategy is also interesting from the chemical point of view, and a good alternative to the direct epoxidation and/or the classical chemical epoxidation methods. Both epoxidation pathways catalyzed by CALB are schematically illustrated in Figure 1.

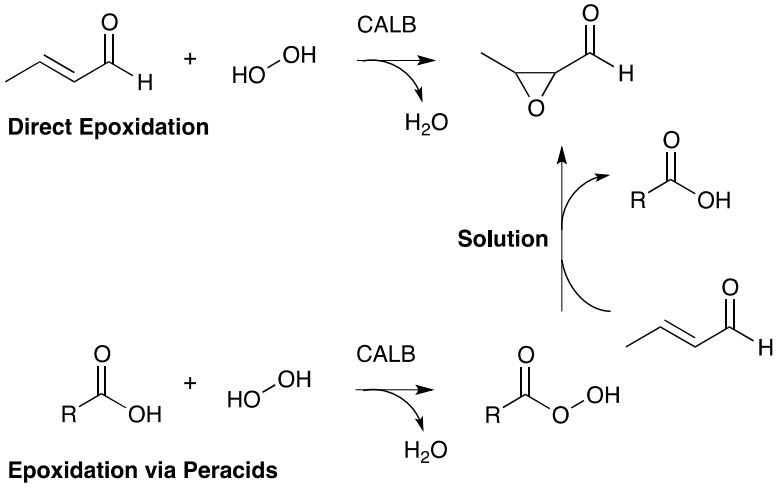

Figure 1. Epoxidation of short alkenes by CALB using two different pathways: the direct epoxidation of alkenes using hydrogen peroxide (top), and the epoxidation of alkenes in solution from peroxy-acids generated by CALB. In this work R- is defined as $(CH_2)_2CH_3$.

In this work, we have focused on the study of the direct epoxidation reaction catalyzed by CALB on short alkenes by means of multiscale quantum mechanics / molecular mechanics (QM/MM) methods, using the Ser105Ala CALB variant to avoid possible undesired hydrolytic activity. 2-butenal served as a substrate for the direct epoxidation reaction, and hydrogen peroxide was chosen as an oxidant due to its mild environmental character, availability and solubility which permits the use of very low concentrations. The selection of this particular oxidant molecule was additionally dictated by the fact that CALB has been reported to tolerate moderate concentrations of hydrogen peroxide.[20,21]

As mentioned above, apart from this enzymatic approach, epoxidation of alkenes can be also achieved through the epoxidation of peroxy-acids in solution. Here the main question arises: which is the most efficient way to produce epoxides in terms of catalytic performance, the enzymatic approach via direct epoxidation or the chemical synthesis using peroxy-acids? In this work, we have also studied the Prilezhaev reaction in organic solvent using a short peroxy-acid of four carbons as a model (perbutyric acid). Comparison of the free energy landscape for the two reactions can indicate which of the studied epoxidation pathways can be an environmentally friendly alternative for the production of epoxides. In a general way, the results of this work also provide general information about the molecular mechanism employed by promiscuous enzymes.

COMPUTATIONAL METHODS

Systems set up. Initial coordinates of the protein were obtained from the PDB structure of *Candida Antarctica* Lipase B (PDB ID: 1TCA).[30] Mutation of the catalytic Ser105 to Ala was done using Mutator plugging in VMD.[31] The corresponding substrates, 2-butenal and hydrogen

peroxide, were built using MOLDEN software[32] into the active site pocket of the pre-equilibrated CALB.[22] 2-butenal was built manually using as an anchor atom the carbonyl oxygen of the substrate studied in previous works.[22] Hydrogen peroxide was built using a water molecule as an anchor that lied in a suitable position in the vicinity of the catalytic diad, especially focusing on its proper orientation towards His224 whose role is its activation, and electrophilic center that will be attacked. The protonation state of titratable residues were determined at pH 7 using the PropKa ver. 3.0.3 program.[33,34] Asp134 with pKa of 7.6 was protonated in OD2 position and only one histidine present in the protein, the catalytic His224, was treated as neutral with hydrogen atom added in Nδ position. Three disulphide bridges were identified between residues Cys22 and Cys64, Cys216 and Cys258, and Cys293 and Cys31. Afterwards, all missing hydrogen atoms were added to the structure and the system was solvated into a 100 × 80 × 80 $Å^3$ pre-equilibrated box of TIP3P[35] water molecules. Water molecules with an oxygen atom within 2.8 Å of any heavy atom were removed. The total charge of the system was zero therefore no counterions were added. The full system was minimized by a series of optimization algorithms, as described elsewhere.[22] Such prepared model was composed by a total of 64045 atoms, from which 4624 correspond to the protein residues, 59406 to water molecules, and 15 to the substrates.

After initial energy minimizations, the system was heated to 303 K with 0.1 K temperature increment and equilibrated during short (100 ps) NPT MD simulations, followed by non-accelerated classical 200 ns NVT MD simulations with AMBER force field,[36] as implemented in NAMD software.[37] According to the time evolution of the RMSD, the system can be considered as equilibrated (Supporting Information Figure S1). The missing force field parameters for the substrates were generated using GAFF[38] and Antechamber[39] tool (Supporting Information Tables S1 and S2). Partial charges were computed using the Austin Model 1 (AM1)[40] semiempirical

Hamiltonian as implemented in Antechamber. During 200 ns non-biased NVT MD simulations with a time step of 1fs, all atoms were free to move within periodic boundary conditions and cut-offs for nonbonding interactions with an internal cut-off of 14.5 Å and an external of 16 Å. In order to avoid diffusion of the substrates, a restrain in the position between the oxygen of the aldehyde and the oxyanion hole, and the hydrogen of the hydrogen peroxide and the NE2 of the catalytic His224, were set up. The Langevin thermostat[41] was used. The relative orientation of the 2-butenal along the dynamics was analyzed by measuring the angle formed by the His224 ring, the asymmetric carbon of the substrate and the hydrogen atom bonded to it. The values were normalized and clustered in using K-Means[42] clustering in order to divide the sample into the geometries that could lead to (R)- and (S)- enantiomers. Two snapshots of the equilibrated system were extracted from the MD trajectory, taking into account that the initial geometry of the substrates could lead into the two possible enantiomers, (R)- and (S)-, i.e. a structure which relative orientation was close to 0 and another close to 1 for (R)- and (S)- respectively. The selected structures were then used for QM/MM calculations after minimization of the full system using a combination of conjugate gradient[43] and L-BFGS-B[44] algorithms, as implemented in fDynamo[45] library.

In order to carry out the QM/MM simulations, the system was divided into two subsets of atoms. The QM region was described at density functional theory (DFT) level using the B3LYP[46,47] functional and the standard 6-31+G(d,p) basis set, as implemented in Gaussian09.[48] It was composed by the lateral chains of the catalytic His224 and Asp187 residues, as well as the full substrates, i.e. 2-butenal and hydrogen peroxide (34 atoms) as shown in Figure 2. In order to saturate the valence between QM and MM boundary two link atoms[49] were placed between Cα-Cβ of side chains of His224 and Asp187. The remaining atoms of the system were treated by the

OPLS-AA[50] and TIP3P[35] force fields for the protein and water molecules, respectively. A truncation function (shift function) was applied to treat the nonbonded interactions, with an internal cut-off defined at 14.5 Å and an external at 16 Å.

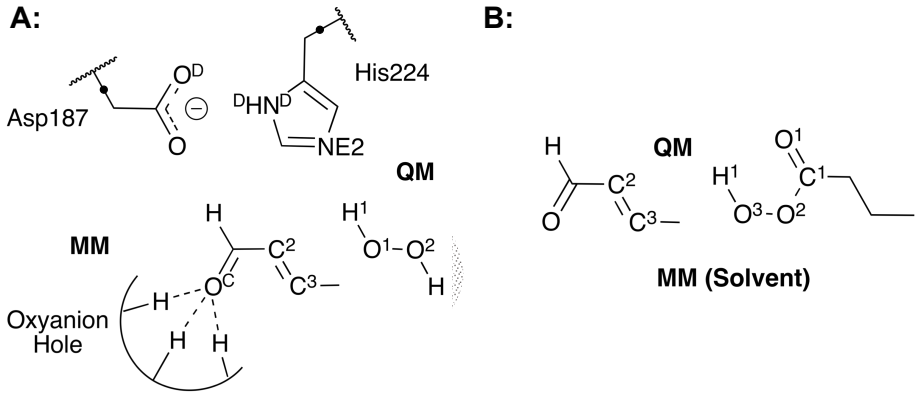

Figure 2. Schematic representation of QM partition. A: CALB active site and its QM sub-set represented as a shaded region. Black dots represent link atoms introduced between QM and MM region. B: QM region for the epoxidation reaction using peroxy-acids in chloroform. The solvent was treated as MM.

For the study of the Prilezhaev reaction in chloroform, both substrates, perbutyric acid and 2-butenal, were solvated with an 80 x 80 x 80 Å^3 solvation box of chloroform molecules. A short classical MD simulation of 5 ns using the NVT ensemble was done in order to equilibrate the box of chloroform using the same approach as described above at 303 K. The substrates were treated at DFT level, as in the case of the reaction in the enzyme. Parameters to describe the chloroform molecules were taken from Amber parameter database.[51] Parameters to describe perbutyric acid were computed following the same procedure as describe before using GAFF and

Antechamber (Supporting Information Table S3). The system consists of 10001 atoms (26 atoms for the substrates and 9975 to chloroform molecules).

Localization of Structures at B3LYP/MM level. Transition state structures for each system were located at B3LYP/MM level using Baker's algorithm[52] using Gaussian09 combined with fDynamo library. Convergence tolerance for localization of structures was set to 1.2 $kJ \cdot mol^{-1} \cdot Å^{-1}$. Subsequently, Hessian was calculated for the optimized structures in order to confirm the nature of the TS structure, yielding only one negative eigenvalue. Then, minimum energy paths from the localized TSs structures were traced using the IRC method. 200 iterative steps in both directions were done with a step of 0.1 Å. Geometry of reactants, intermediates and products from the IRC were optimized using the same Baker's algorithm with a 1.2 $kJ \cdot mol^{-1} \cdot Å^{-1}$ convergence.

Free Energy Calculations. In order to obtain the free energy landscape of the reactions Free Energy Perturbation (FEP) method was used.[53,54] FEP requires the sampling of the environment over a previously traced IRC down to RS and PS from the TS, in our case at B3LYP/MM level of theory. For this reason, the free energy profile is obtained over a realistic reaction coordinate. In this case the MM charges of the environment polarize the wave function of the QM part and permits the exploration of the reaction path at high level of theory.

The structures used in FEP calculations were extracted from the traced IRC, and are characterized by a single *s* coordinate

(1)

where , and are the coordinates of the *i*th structure and *j*th QM atom of the structure, and are the corresponding masses of the QM atoms.

So, the free energy relative to reactants can be expressed as a function of *s* as presented in equation 2:

(2)

where is the gas-phase energy of the QM sub-set computed at DFT level, ZPE is the zero-point energy, k_B is the Boltzmann constant and T is the temperature. QM/MM contribution to the free energy between two values of is calculated by averaging the QM/MM interaction energy over all the MM atoms obtained during the molecular dynamics (MD) simulation. In particular, 20 ps of QM/MM MD simulation were done for each window along the IRC path at 293 K using the NVT ensemble, maintaining the QM subset frozen during the simulation. The total amount of windows employed to generate the full energy path was 49 and 108 for first and second steps taking place in the active site of CALB in the case of (R)-enantiomer, 51 and 113 for (S)-enantiomer, and 88 windows to study the chemical transformation of the peroxy-acid in chloroform, respectively. Free energy between the solvated separated substrates in solution and the reactants complex (RC) was estimated using the SMD[55] Continuum Solvation Model. Finally in order to take into account dispersion effects produced by the oxyanion hole, empirical dispersion was considered by computing single point calculations along the IRC using the empirical DFT-D3(BJ)[56,57] as implemented in Gaussian09. Statistical errors to the FEP calculations were computed by means of first-order expansion, as proposed by Chipot[58] (Supporting Information Tables S4 and S8).

Binding Free energy. In order to evaluate the interaction energy between the substrates and the protein, alchemical free perturbation method has been applied as described in previous works.[59–61] A series of QM/MM MD were carried out in the enzyme-substrate complex in the

Michaelis complex state, and in the substrate solvated in a box of water molecules. The QM subset of atoms, consisting in this case on just the substrates, was treated by the Austin Model 1 (AM1)[40] semiempirical Hamiltonian with the standard 6-31+G(d,p) basis set. Two parameters λ and γ were introduced in the electrostatic and van der Waals interaction terms respectively, as showed in equation 3:

(3)

Then, changes were smoothly introduced in λ and γ parameters from 1 to 0 in order to annihilate the electrostatic and van der Waals interaction contributions. The calculation of the free energy difference between two consecutive steps is obtained, and then the total free energy change is obtained by the sum of all the contribution between all the steps covering the whole transformation from the initial to the final states. Here we used a total of 100 windows to evaluate the electrostatic and van der Waals interaction term, with a step for λ and γ of 0.01 (from 1 to 0). In each window a total of 20 ps of AM1/MM MD at 293 K were performed using the NVT ensemble. Finally, the binding free energy can be computed as the difference between ΔG_W in the water solvent and ΔG_E in the Michaelis complex.

(4)

Kinetic Isotope Effects. KIEs were calculated from isotopic substitution of the key atoms from localized RS and TS structures. From the definition of the free energy of a state and using the Transition State Theory,[62] the ratio between the rate constants corresponding to the heavy and the light atoms can be computed by means of

(5)

where, Q refers to the total partition function which was computed as the product of the translational, rotational and vibrational partition functions of isotopologs in RS and TS structures, and ΔZPE refers to difference of the zero point energy between RS and TS in the light (L) and heavy (H) isotopologs.[63,64] KIEs were computed at B3LYP/MM level of theory and one RS structure and one TS structure for each step of the reaction were used to compute the KIE. The Hessian matrixes were computed for the QM subset of atoms.

RESULTS AND DISCUSSION

Direct epoxidation catalyzed by CALB. As mentioned in previous sections, a short alkene 2-butenal has been used as a model of substrate in this study. A previous study for the direct epoxidation by hydrogen peroxide, derived from a computational study based on a reduced cluster model to mimic the active site of CALB,[20] suggested that the reaction takes place in two steps, as shown in Figure 3. According to this proposal, we explored the two chemical steps by means of QM/MM FEP methods with the full enzyme solvated in a box of water molecules. The first step involves the attack of the oxygen (O^1) of the hydrogen peroxide to the carbon (C^3) of the alkene, concomitant with the proton transfer from the oxygen (O^1) to His224. In this first step, a negative charge is developed in the carbonyl oxygen atom of the substrate, which is stabilized by the oxyanion hole formed by Thr40 and Gln106. The role of this oxyanion hole is well known and has been stated in other reactions catalyzed by CALB.[22–24,65] The formation of the epoxide ring by the bond forming between C^2 and O^1 takes place in the second step. This second step is assisted by the acid/base character of the His224 that permits the transfer of the proton H^1 to the oxygen O^2 thus forming a water molecule.

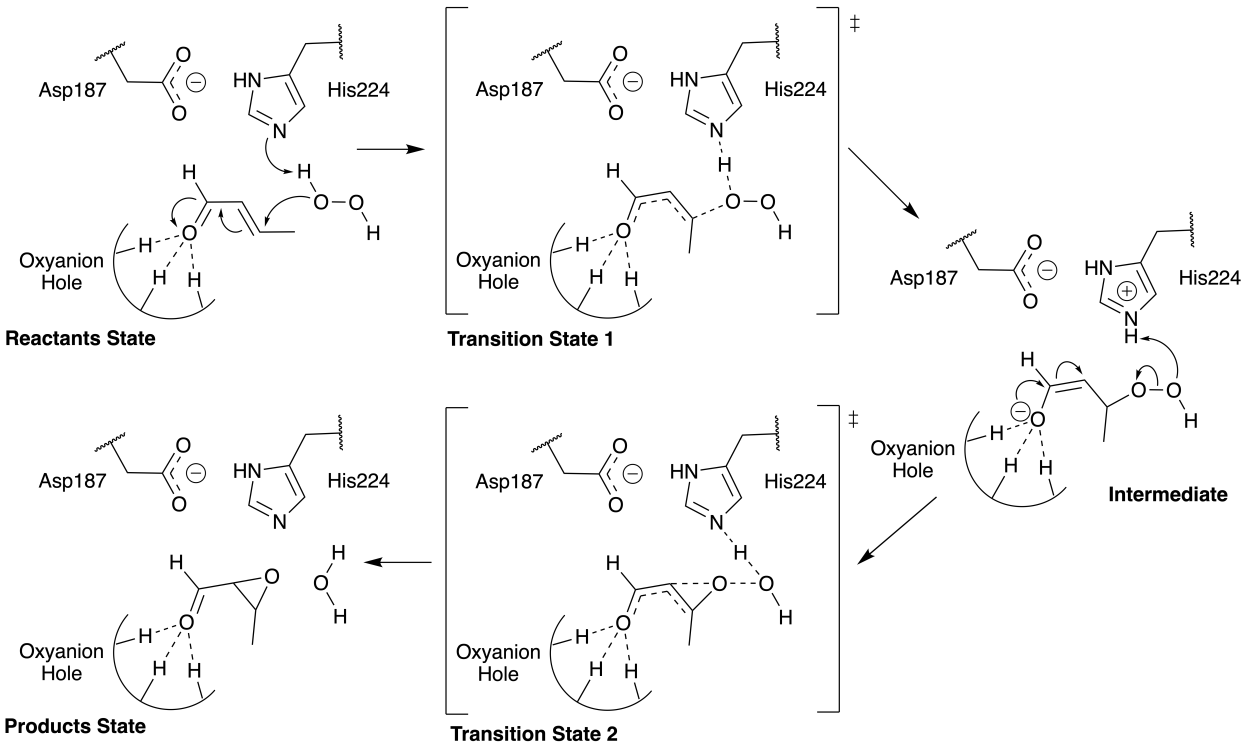

Figure 3. Schematic representation of the reaction mechanism of the direct epoxidation of 2-butenal with hydrogen peroxide catalyzed by CALB.

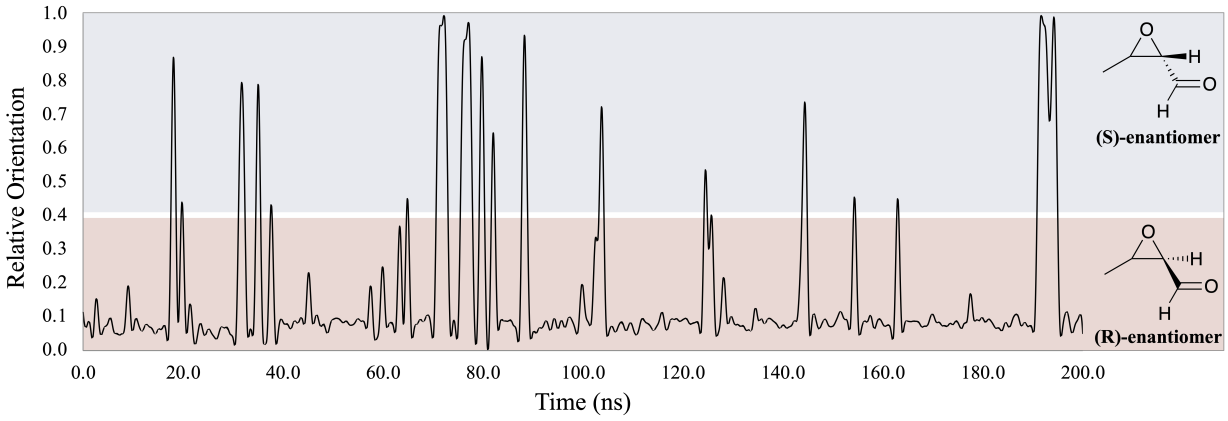

Figure 4. Relative orientation of the substrate 2-butenal along 200 ns of classical MD. Baseline 0.0 corresponds to (R)-enantiomer and 1.0 is the corresponding (S)-geometry. Cutoff between R- and S- geometry was computed applying K-Means clustering.[42]

Due to the nature of this short alkene and the presence of an asymmetric carbon atom in the products of the reaction, C^2, two different enantiomers can be formed, as shown in Figure 4, which is dictated by the relative orientation of both substrates, 2-butenal and hydrogen peroxide, in the reactants state. This relative orientation is determined by the 2-butenal pose established in the active site. Thus, possible orientations of this substrate were explored during a 200 ns classical MD. The orientation of the substrate that will determine the final (R)- epoxide is represented as values close to 0, while relative orientation values around 1 lead to (S)- epoxide. As Figure 4 indicates, although both orientations were identified along the MD trajectory, (R)-like geometry seem to be the dominant one (90.9 % of overall explored structures). Similar results were obtained when starting the MD simulation from the (S)- enantiomer (Supporting Information Figure S2). Interestingly, analysis of the interaction energies between the two possible conformations of the substrate and the protein reveals that there is no single evident interaction that can explain the results, but a global effect of the protein (Supporting Information Figure S3). Nevertheless, this result can not be considered as a final conclusion about the propensity of obtaining one or the other enantiomer and exploration of the subsequent chemical reaction is required. Once the substrate binds to the active site, the rotation around the C^1-C^2 bond is restricted, and this fact leads to the formation of one or other enantiomer because of the defined relative orientation of the alkene and the hydrogen peroxide. Since this fact is *a priori* very attractive from the biocatalytic point of view, both possible mechanisms were studied. The resulting free energy profiles are shown in Figure 5, average structures of the key states appearing along the reaction are presented in Figure 6 and 7, while key distances and charges of localized structures of reactants state (RS), TSs, intermediates (INT) and product states (PS) are deposited in the Supporting Information.

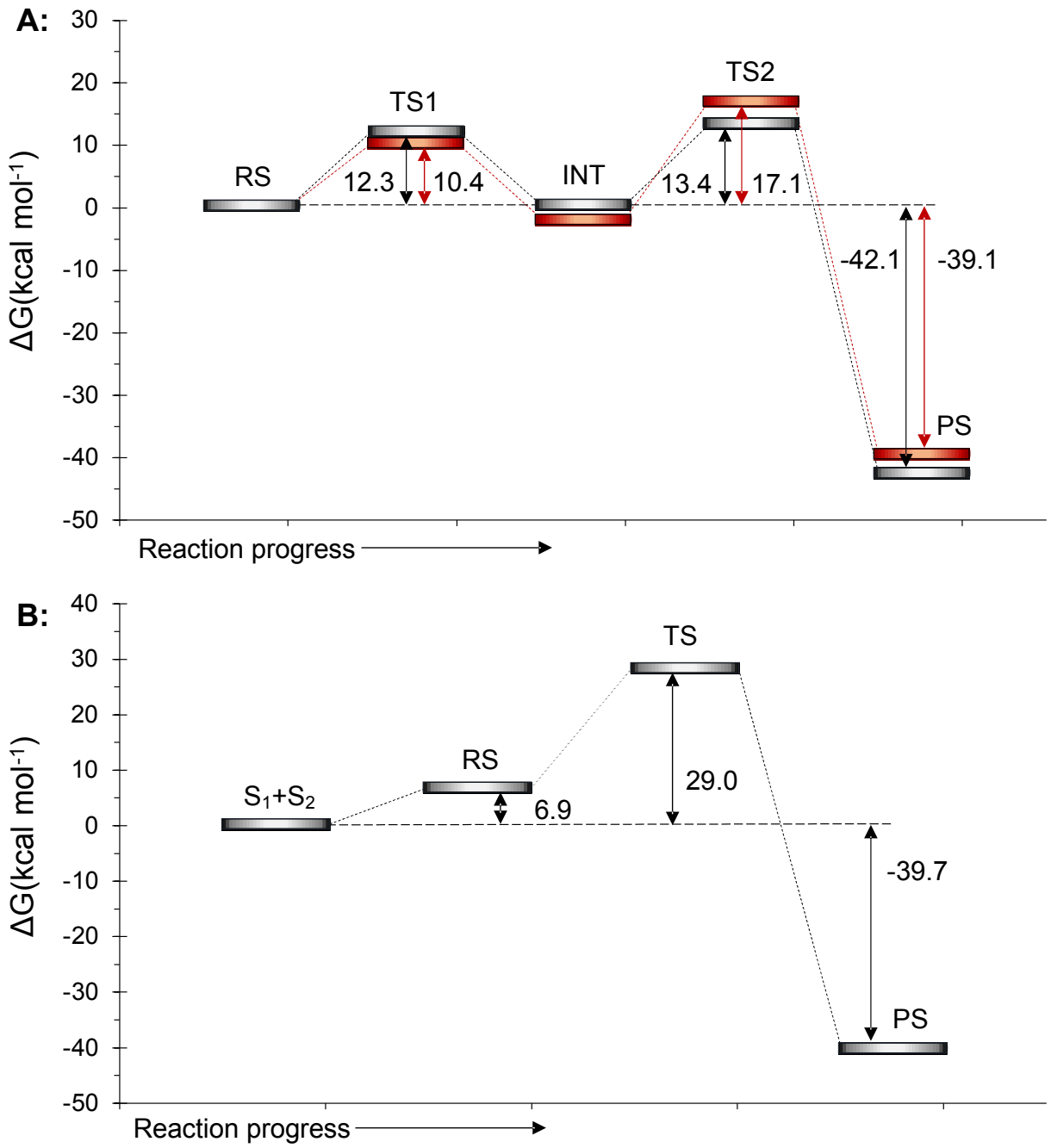

Figure 5. B3LYP-D3(BJ)/MM free energy profile of the epoxidation of 2-butenal. Panel A corresponds to the reaction catalyzed by CALB to render the (R)- (red line) and (S)- (grey line) epoxide enantiomers, while panel B shows the epoxidation of 2-butenal by perbutyric acid in chloroform.

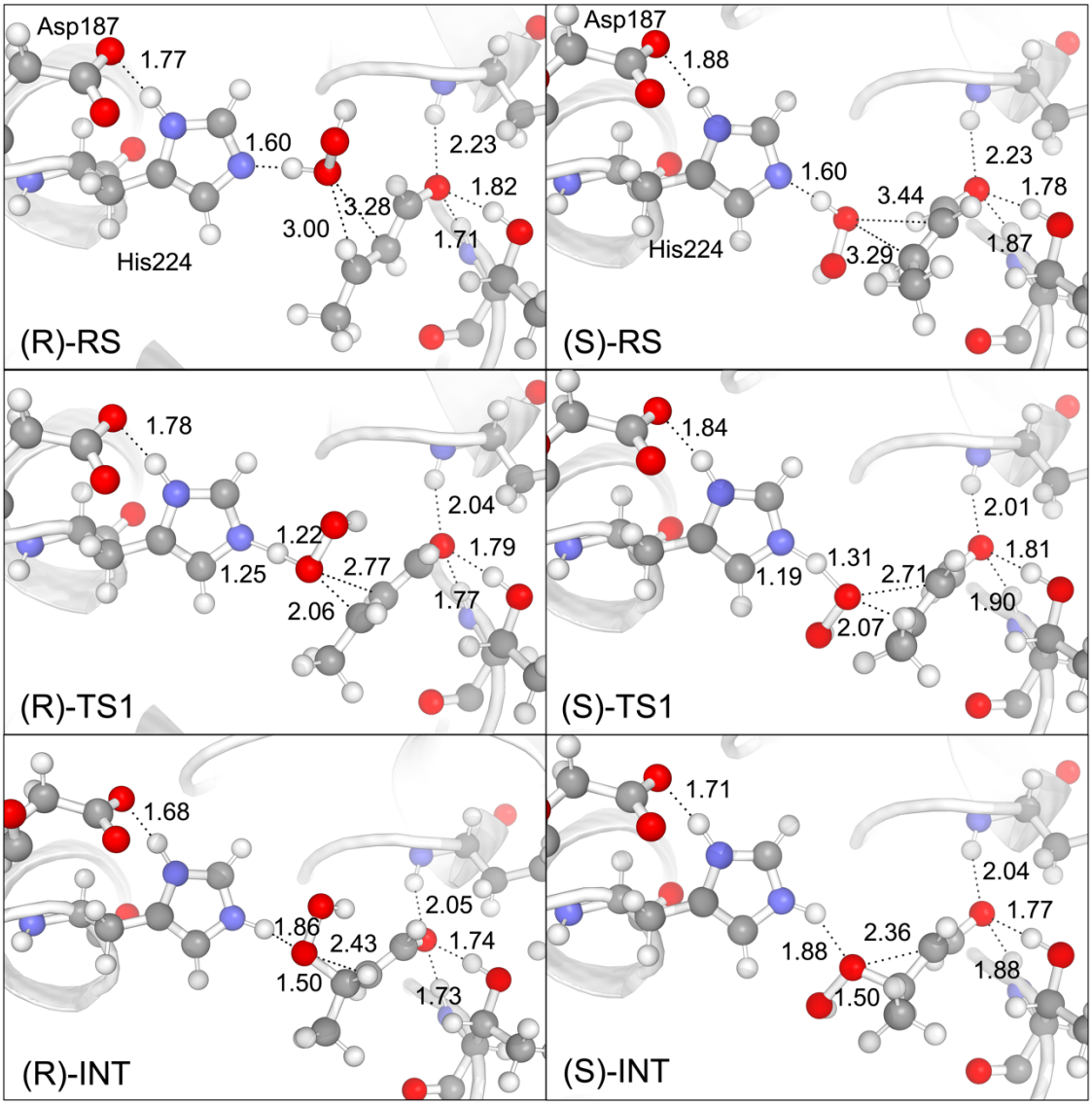

Figure 6. Representative structures of the state localized at B3LYP/MM level of the first step of the direct epoxidation of 2-butenal with hydrogen peroxide catalyzed by CALB. Left panel corresponds to (R)- enantiomer and right panel to (S)- enantiomer. Key residues and substrates are shown in ball and sticks representation. All distances are in Å.

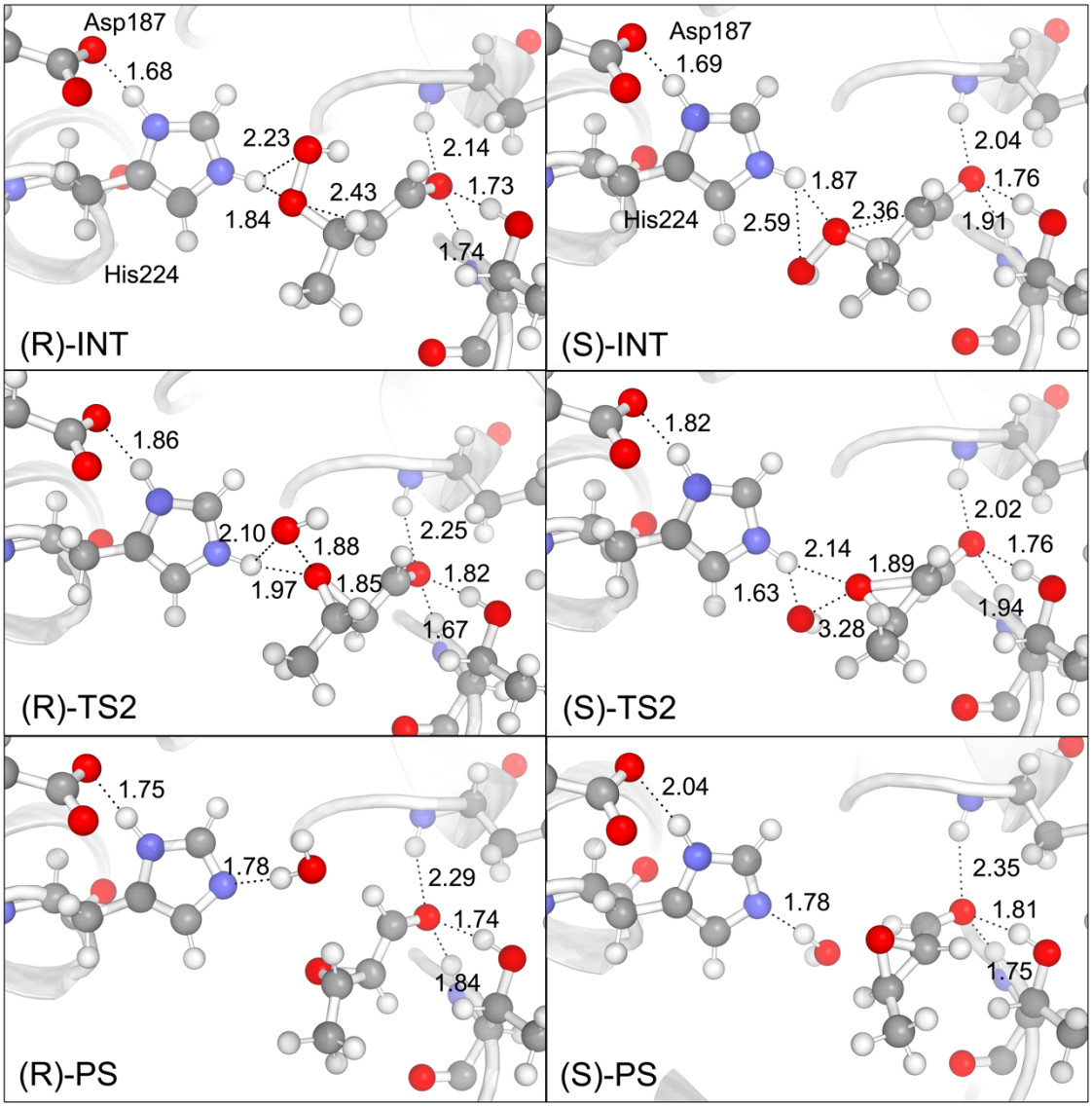

Figure 7. Representative structures of the state localized at B3LYP/MM level of the second step of the direct epoxidation of 2-butenal with hydrogen peroxide catalyzed by CALB. Left panel corresponds to (R)- enantiomer and right panel to (S)- enantiomer. Key residues and substrates are shown in ball and sticks representation. Distances are in Å.

The analysis of the free energy profiles of the chemical steps of the process catalyzed by CALB, as depicted in Figure 5, and the geometrical analysis of the structures obtained along the reaction, pathway as illustrated in Figures 6 and 7, confirms the proposed two-step mechanism

and show that the formation of (S)- enantiomer is kinetically and thermodynamically more favorable than formation of (R)-enantiomer. The experimentally measured rate constant k_{cat} of 0.56 s^{-1} [20] that, within the framework of the Transition State Theory[62] corresponds to a free energy of barrier of 17.5 kcal·mol^{-1} at 293 K, is in between the values computed for the (R)- and (S)-enantiomers at 298 K. Experiments performed by Brinck and co-workers suggested that this reaction leads to a racemic mixture without a preference towards any enantiomer showing no enantioselectivity.[20] Considering the differences in the activation and reaction energies for the formation of both products deduced from our simulations (3.7 and 3.0 kcal·mol^{-1}, respectively) the experimental results would not match with our reactivity results if the reaction was carried out either under kinetic or thermodynamic control.

In general, despite no significant geometrical differences are detected between the geometries of the different states of both paths, the different reactivity between (R)- and (S)- enantiomers can be rationalized based on the different relative orientation of the substrate in the INT and TS2. Thus, the C2-O1 distance in the (S)-INT is slightly shorter than in the (R)-INT enantiomer (2.36 vs 2.43 Å). This, together with a longer distance in the (S)-TS2 than in the (R)-TS2 (1.89 vs 1.85 Å) implies a larger variation of this reaction coordinate from INT to the TS2 in the (R)- than in the (S)- conformer (0.58 vs 0.47 Å) which is in agreement with a larger activation free energy. According to these results, TS2 is closer to the INT in the (S)- than in the (R)-, which is in agreement with the Hammond postulate that predicts TSs closer to reactants for those reactions with low activation energies and large reaction energies, as it is the case when comparing the energy profile for the (R)- and the (S)- conformers. Regarding the H1 transfer from NE2 to O2, a different scenario is obtained. Thus, H1-O2 distance is 1.84 and 1.88 Å in the (R)- and (S)- INT, respectively. This would suggest a slightly better conformation for the proton transfer in the (R)-

conformer, taking into account that H1-O2 is the bond to be formed in this step. Nevertheless, the stronger interaction established between the transferring H1 atom and O1 in (R)-TS2, by comparison with the (S)-TS2 (1.97 and 2.14 Å, respectively) provokes a delay in the H1 transfer from NE2 to O2 in the (R)- (H1-O2 distance equal to 2.10 Å in TS2), by comparison with the (S)- conformer (H1-O2 distance equal to 1.63 Å in TS2). In fact, the larger accumulation of negative charge on the O2 atom in the (R)-TS2 than in the (S)-TS2 (-0.794 and -0.692 a.u., respectively, as shown in Supporting Information) is in agreement with these detected geometrical differences that explains the different computed energy barriers.

The geometrical analysis of the inter-atomic distance between the substrate and the active site also shows the role of the Asp187-His224 diad, or the oxyanion hole formed by residues Thr40 and Gln106. Thus, in general, the shortest distances between O^{c} and the H^{Thr40} and H^{Gln106} are detected in the INT, where the charge on O^{c} reaches the most negative value (see Table S5, S6 and S7 in Supporting Information).

Kinetic Isotope Effects. In order to compute other magnitudes that could be directly compared with experiments to confirm the proposed results, kinetic isotope effects (KIEs) were computed for the CALB catalyzed reactions rendering the R and S enantiomers. KIEs were computed with TS1 and TS2, in an attempt to identify any difference in either the first or the second steps and assuming that intrinsic KIEs can be measured for this reaction. According to the values reported in Table 1 and, taking into account the uncertainty associated to the method, the KIEs obtained for the R and S enantiomers can be considered as equivalent.

Table 1. KIEs computed at B3LYP/MM level for the direct epoxidation of 2-butenal catalyzed by CALB.

	Enantiomer R		Enantiomer S	
	TS1	TS2	TS1	TS2
[2-^{14}C]	1.011	0.972	1.017	0.980
[3-^{14}C]	1.017	1.058	1.001	1.034
[1-^{18}O]	0.990	1.046	1.031	1.046
[2-^{18}O]	0.994	1.010	0.994	1.030

Substrate-enzyme binding step. Once analyzed the chemical reaction steps, it must be taken into account that the overall catalytic efficiency is dictated not only by the k_{cat}, but also by the ability of the substrate to bind into the enzyme cavity, K_M. In order to get information about this crucial step that defines the pose of the substrate that will lead to one or another enantiomer, binding free energies ΔG_{bind} were calculated by means of alchemical FEP methods. Binding free energies were computed as the difference of electrostatics and van der Waals contributions between the substrate in the Michaelis Complex (MC) in the active site of the protein, and the solvated reactants in solution. As shown in Table 2, a difference of $\Delta G_{bind(R)}$ -$\Delta G_{bind(S)}$ of 2.1 kcal·mol^{-1} was found between the geometries that will lead to the two enantiomers. This value suggests that R orientation would bind the active site with slightly higher probability than S orientation, which is in agreement with the selectivity that can be deduced from the population analysis of the MC complexes based on classical MD simulations (see Figure 4), but in contrast with the predicted trend emerged from the difference in the chemical catalytic performance of the two systems, R and S, as studied above.

Table 2. Binding free energy computed at AM1/MM of 2-butenal into the active site of CALB to generate, after the chemical reaction, the two (R)- and (S)-enantiomers of the epoxide. Electrostatic and van der Waals contributions are given separately. Energies are given in kcal·mol^{-1}.

	Solution	Geometry for (R)-enantiomer		Geometry for (R)-enantiomer	
		RC	ΔG_E-ΔG_W	RC	ΔG_E-ΔG_W
Elec.	-6.99 ± 0.13	-9.22 ± 0.09	-2.23 ± 0.15	-8.1 ± 0.11	-1.11 ± 0.17
vdW	-9.86 ± 0.03	-16.26 ± 0.03	-6.4 ± 0.05	-15.27 ± 0.02	-5.41 ± 0.04
Total	-16.9 ± 0.13	-25.5 ± 0.09	-8.6 ± 0.16	-23.4 ± 0.11	-6.5 ± 0.17

Epoxidation reaction in solution. In order to answer the question of whether the most efficient way to produce epoxides, in terms of catalytic performance, is the enzymatic approach via direct epoxidation or the chemical synthesis using peroxy-acids, the Prilezhaev reaction was studied in chloroform as proposed in previous studies.[66] A short peroxy-acid, perbutyric acid, was used as model as suggested in previous works.[67,68] The reaction goes through what is called a butterfly mechanism, as depicted in Figure 8. The study of the reaction at B3LYP/MM level shows that it occurs in a single step where the transfer of the proton H^1 towards the carbonyl oxygen O^1 of the peroxy-acid takes places concomitant with the peroxy-acid oxygen O^3 attack to the carbon of the alkene, the closing of the epoxide ring between C^2-C^3 of the 2-butenal and the formation of butyric acid. Key interatomic distances and atomic charges for localized states for the reaction are shown in Table S9 and Table S10 in Supporting Information.

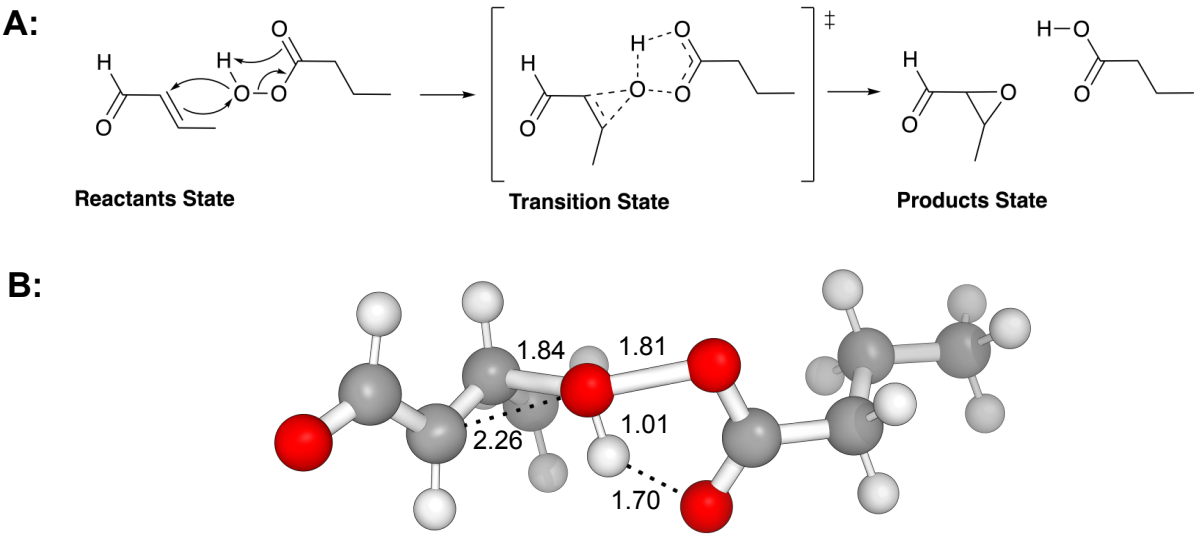

Figure 8. A: Schematic representation of the epoxidation of 2-butenal by perbutyric acid in solution. B: Representation of the TS structure of the reaction in chloroform, as obtained at B3LYP/MM level.

From the energetic point of view, both enantiomers are equally probable when the reaction takes place in solution, since the specific solvent-substrate interaction in both enantiomers are indistinguishable. The free energy profiles of the reaction, also studied using FEP methods, are shown in Figure 5. As observed, the obtained energy barrier, 29.0 kcal·mol^{-1}, is significantly higher than the values obtained when reaction is catalyzed by the enzyme. The barrier is too high for this reaction to take place in a reasonable timescale and, consequently, the use of this reaction in solution must be discarded, by comparison with the alternative enzymatic approach, as a green strategy to get epoxides.

CONCLUSIONS

In this paper, we present a QM/MM computational study of the epoxidation of alkenes catalyzed by the Ser105Ala CALB enzyme and compared with the alternative epoxidation of alkenes by peroxy-acids in chloroform. Free energy profiles obtained with FEP methods at B3LYP/MM level show how the epoxidation of 2-butenal catalyzed Ser105Ala CALB takes place in a two steps manner. The first step involves the attack of one of the oxygens of the hydrogen peroxide (O^1) to one of the carbon atoms of the double bond of the alkene (C^3), concomitant with the proton transfer from the same oxygen atom (O^2) to His224. The closing of the epoxide ring between takes place in the second step, which is assisted by the acid/base character of the His224 that permits the transfer of the proton H^1 to the oxygen O^2 thus forming a water molecule. The calculations show how the negative charge developed in the carbonyl oxygen atom of the substrate is stabilized by the oxyanion hole formed by Thr40 and Gln106. The presence of an asymmetric atom on the substrate opens the possibility of two different enantiomeric products. A deep analysis of the evolution of the geometries and charges in the active site of the enzyme along the reaction reveals how the relative orientation of the substrate, when producing the (S)- enantiomer, facilitates the presence of intermolecular interactions that increase the reactivity of the substrate to form the peroxide ring in the second step. The active site His224 residue, posed closer to the substrate when generating the (R)- enantiomer, interacts by means of a strong hydrogen bond with the attacking oxygen (O^1) of the hydrogen peroxide oxygen atom, thus reducing its negative charge and provoking an increase of the energy barrier. The exploration of the free energy landscape of the chemical steps of the full process catalyzed by Ser105Ala CALB suggests that the enzyme should show enantioselectivity favoring the S enantiomer. Nevertheless, either the population analysis of the two possible orientations of the

substrate in the active site, based on unbiased MD simulations, and the study of the protein-substrate binding step, explored by means of alchemical FEP methods, dictate a possible (R)-enantioselectivity. Thus, the R- enantioselectivity that would be dictated by the binding step and the preference for the (S)-enantiomer derived from the chemical step of the full catalyzed process could cancel out, thus rendering the lack of enantioselectivity experimentally observed.

According to our results, the alternative route to get the epoxides in chloroform, the Prilezhaev reaction, would take place in a single step, but with a significantly higher free energy barrier. Thus, our results support the use of a promiscuous modified Ser105Ala CALB enzyme as an environmentally friendly alternative for the production of epoxides in industry. Further re-designs of the enzyme could be studied in the future to increase the efficiency of the biocatalyzed process.

ASSOCIATED CONTENT

The Supporting Information is available free of charge at x:

Free energy surfaces of all mechanisms, key distances and charges tables, evolution of the RMSD during MD, substrate-protein interaction energies for the (R)- and (S)- 2-butenal isomers, and parameters of the substrates.

AUTHOR INFORMATION

Corresponding Author

*Dr. Katarzyna Świderek, e-mail: swiderek@uji.es

*Prof. Vicent Moliner, e-mail: moliner@uji.es

Author Contributions

M. A. Galmés carried out all the calculations, K. Świderek and V. Moliner designed the project and analyzed the results. All authors contributed to writing the manuscript.

Funding Sources

This work was supported by the Spanish Ministerio de Ciencia e Innovación (grant PGC2018-094852-B-C21 and PID2019-107098RJ-I00), the Generalitat Valenciana (grant AICO/2019/195 and SEJI/2020/007) and Universitat Jaume I (grant UJI·B2017-31 and UJI-A2019-04).

ACKNOWLEDGMENT

We would like to thank the Spanish Ministerio de Ciencia e Innovación (grant PGC2018-094852-B-C21 and PID2019-107098RJ-I00), the Generalitat Valenciana (grant AICO/2019/195 and SEJI/2020/007) and Universitat Jaume I (grant UJI·B2017-31 and UJI-A2019-04). MAG thanks Universitat Jaume I for FPI-UJI grant (PREDOC/2017/23). Authors acknowledge computational resources from the Servei d'Informàtica of Universitat Jaume I.

DATA AND SOFTWARE AVAILABILITY

1TCA PDB structure can be downloaded from www.rcsb.org/structure/1TCA

VMD v1.9.2 can be downloaded free of charge from www.ks.uiuc.edu/Research/vmd

NAMD v2.14 can be downloaded free of charge from www.ks.uiuc.edu/Research/namd

PROPKA3 v3.2 can be freely downloaded from github.com/jensengroup/propka

MOLDEN v5.8.1 can be downloaded under academic license from www3.cmbi.umcn.nl/molden

Antechamber is part of AmberTools20 that can be get from ambermd.org/AmberTools.php

Gaussian 09 D01 can be purchased from gaussian.com

fDYNAMO v2.2 can be freely downloaded from www.pdynamo.org/downloads

REFERENCES

(1) Gotor-Fernández, V.; Brieva, R.; Gotor, V. Lipases: Useful Biocatalysts for the Preparation of Pharmaceuticals. *J. Mol. Catal. B Enzym.* **2006**, *40*, 111–120.

(2) Busto, E.; Gotor-Fernández, V.; Gotor, V. Hydrolases: Catalytically Promiscuous Enzymes for Non-Conventional Reactions in Organic Synthesis. *Chem. Soc. Rev.* **2010**, *39*, 4504–4523.

(3) Tawfik, D. S.; Khersonsky, O. Enzyme Promiscuity: A Mechanistic and Evolutionary Perspective. *Annu. Rev. Biochem.* **2010**, *79*, 471–505.

(4) Sheldon, R. A.; Brady, D. The Limits to Biocatalysis: Pushing the Envelope. *Chem. Commun.* **2018**, *54*, 6088–6104.

(5) Leveson-Gower, R. B.; Mayer, C.; Roelfes, G. The Importance of Catalytic Promiscuity for Enzyme Design and Evolution. *Nat. Rev. Chem.* **2019**, *3*, 687–705.

(6) Rix, G.; Watkins-Dulaney, E. J.; Almhjell, P. J.; Boville, C. E.; Arnold, F. H.; Liu, C. C. Scalable Continuous Evolution for the Generation of Diverse Enzyme Variants Encompassing Promiscuous Activities. *Nat. Commun.* **2020**, *11*, 5644.

(7) Sheldon, R. A.; Brady, D. Broadening the Scope of Biocatalysis in Sustainable Organic Synthesis. *ChemSusChem* **2019**, *12*, 2859–2881.

(8) Prileschajew, N. Oxydation Ungesättigter Verbindungen Mittels Organischer Superoxyde. *Berichte der Dtsch. Chem. Gesellschaft* **1909**, *42*, 4811–4815.

(9) Bartlett, P. D. Recent Work on the Mechanisms of Peroxide Reactions. *Rec. Chem. Prog.*

1905, *11*, 47–51.

(10) Plesnicar, B.; Tasevski, M.; Azman, A. The Transition State for the Epoxidation of Ethylene with Peroxyformic Acid. An Ab Initio Molecular Orbital Study. *J. Am. Chem. Soc.* **1978**, *100*, 743–746.

(11) Singleton, D. A.; Merrigan, S. R.; Liu, J.; Houk, K. N. Experimental Geometry of the Epoxidation Transition State. *J. Am. Chem. Soc.* **1997**, *119*, 3385–3386.

(12) Azeez, A. A.; Rhee, K. Y.; Park, S. J.; Hui, D. Epoxy Clay Nanocomposites - Processing, Properties and Applications: A Review. *Compos. Part B Eng.* **2013**, *45*, 308–320.

(13) Jin, F. L.; Li, X.; Park, S. J. Synthesis and Application of Epoxy Resins: A Review. *J. Ind. Eng. Chem.* **2015**, *29*, 1–11.

(14) Orellana-Coca, C.; Camocho, S.; Adlercreutz, D.; Mattiasson, B.; Hatti-Kaul, R. Chemo-Enzymatic Epoxidation of Linoleic Acid: Parameters Influencing the Reaction. *Eur. J. LIPID Sci. Technol.* **2005**, *107*, 864–870.

(15) Scotti, N.; Ravasio, N.; Psaro, R.; Evangelisti, C.; Dworakowska, S.; Bogdal, D.; Zaccheria, F. Copper Mediated Epoxidation of High Oleic Natural Oils with a Cumene-O-2 System. *Catal. Commun.* **2015**, *64*, 80–85.

(16) Zhou, P.; Wang, X.; Yang, B.; Hollmann, F.; Wang, Y. Chemoenzymatic Epoxidation of Alkenes with Candida Antarctica Lipase B and Hydrogen Peroxide in Deep Eutectic Solvents. *RSC Adv.* **2017**, *7*, 12518–12523.

(17) Tong, K. H.; Wong, K. Y.; Chan, T. H. A Chemoenzymic Approach to the Epoxidation of Alkenes in Aqueous Media. *Tetrahedron* **2005**, *61*, 6009–6014.

(18) Zaks, A.; Dodds, D. R. Chloroperoxidase-Catalyzed Asymmetric Oxidations - Substrate-Specificity and Mechanistic Study. *J. Am. Chem. Soc.* **1995**, *117*, 10419–10424.

(19) de Visser, S. P.; Ogliaro, F.; Sharma, P. K.; Shaik, S. What Factors Affect the Regioselectivity of Oxidation by Cytochrome P450? A DFT Study of Allylic Hydroxylation and Double Bond Epoxidation in a Model Reaction. *J. Am. Chem. Soc.* **2002**, *124*, 11809–11826.

(20) Humble, M. S.; Carlqvist, P.; Branneby, C.; Allnér, O.; Frise, A.; Hult, K.; Berglund, P.; Brinck, T. Direct Epoxidation in Candida Antarctica Lipase B Studied by Experiment and Theory. *ChemBioChem* **2008**, *9*, 2443–2451.

(21) Wang, X. P.; Zhou, P. F.; Li, Z. G.; Yang, B.; Hollmann, F.; Wang, Y. H. Engineering a Lipase B from Candida Antactica with Efficient Perhydrolysis Performance by Eliminating Its Hydrolase Activity. *Sci. Rep.* **2017**, *7*, 1–5.

(22) Świderek, K.; Martí, S.; Moliner, V. Theoretical Study of Primary Reaction of Pseudozyma Antarctica Lipase B as the Starting Point to Understand Its Promiscuity. *ACS Catal.* **2014**, *4*, 426–434.

(23) Bordes, I.; Recatalá, J.; Świderek, K.; Moliner, V. Is Promiscuous CALB a Good Scaffold for Designing New Epoxidases? *Molecules* **2015**, *20*, 17789–17806.

(24) Świderek, K.; Moliner, V. Computational Studies of Candida Antarctica Lipase B to Test Its Capability as a Starting Point to Redesign New Diels-Alderases. *J. Phys. Chem. B* **2016**, *120*, 2053–2070.

(25) Galmés, M. A.; García-Junceda, E.; Świderek, K.; Moliner, V. Exploring the Origin of

Amidase Substrate Promiscuity in CALB by a Computational Approach. *ACS Catal.* **2020**, *10*, 1938–1946.

(26) Wikmark, Y.; Humble, M. S.; Bäckvall, J. E. Combinatorial Library Based Engineering of Candida Antarctica Lipase a for Enantioselective Transacylation of Sec-Alcohols in Organic Solvent. *Angew. Chemie - Int. Ed.* **2015**, *54*, 4284–4288.

(27) Chen, X. Y.; Chen, G. J.; Wang, J. L.; Wu, Q.; Lin, X. F. Lipase/Acetamide-Catalyzed Carbon-Carbon Bond Formations: A Mechanistic View. *Adv. Synth. Catal.* **2013**, *355*, 864–868.

(28) Sarmah, N.; Revathi, D.; Sheelu, G.; Rani, K. Y.; Sridhar, S.; Mehtab, V.; Sumana, C. Recent Advances on Sources and Industrial Applications of Lipases. *Biotechnol. Prog.* **2018**, *34*, 5–28.

(29) Chávez, G.; Hatti-Kaul, R.; Sheldon, R. A.; Mamo, G. Baeyer–Villiger Oxidation with Peracid Generated in Situ by CaLB-CLEA Catalyzed Perhydrolysis. *J. Mol. Catal. B Enzym.* **2013**, *89*, 67–72.

(30) Uppenberg, J.; Morgens, H.; Shamkant, P.; Alwyn, J. T. The Sequence, Crystal Structure Determination and Refinement of Two Crystal Forms of Lipase B from Candida Antarctica. *Structure* **1994**, *2*, 293–308.

(31) Humphrey, W.; Dalke, A.; Schulten, K. VMD - Visual Molecular Dynamics. *J. Molec. Graph.* **1996**, *14*, 33–38.

(32) Schaftenaar, G.; Noordik, J. H. Molden: A Pre-and Post-Processing Program for Molecular and Electronic Structures. *J. Comput. Aided. Mol. Des.* **2000**, *14*, 123–134.

(33) Olsson, M. H. M.; SØndergaard, C. R.; Rostkowski, M.; Jensen, J. H. PROPKA3: Consistent Treatment of Internal and Surface Residues in Empirical p Kapredictions. *J. Chem. Theory Comput.* **2011**, *7*, 525–537.

(34) Søndergaard, C. R.; Olsson, M. H. M.; Rostkowski, M.; Jensen, J. H. Improved Treatment of Ligands and Coupling Effects in Empirical Calculation and Rationalization of PKa Values. *J Chem Theory Comput* **2011**, *7*, 2284–2295.

(35) Jorgensen, W. L.; Chandrasekhar, J.; Madura, J. D.; Impey, R. W.; Klein, M. L. Comparison of Simple Potential Functions for Simulating Liquid Water. *J. Chem. Phys.* **1983**, *79*, 926–935.

(36) Duan, Y.; Wu, C.; Chowdhury, S.; Lee, M. C.; Xiong, G.; Zhang, W.; Yang, R.; Cieplak, P.; Luo, R.; Lee, T.; et al. A Point-Charge Force Field for Molecular Mechanics Simulations of Proteins Based on Condensed-Phase Quantum Mechanical Calculations. *J. Comput. Chem.* **2003**, *24*, 1999–2012.

(37) Phillips, J. C.; Braun, R.; Wang, W. E. I.; Gumbart, J.; Tajkhorshid, E.; Villa, E.; Chipot, C.; Skeel, R. D.; Poincare, H. Scalable Molecular Dynamics with NAMD. *J. Comput. Chem.* **2005**, *26*, 1781–1802.

(38) Wang, J.; Wolf, R. M.; Caldwell, J. W.; Kollman, P. A.; Case, D. A. Development and Testing of a General Amber Force Field. *J. Comput. Chem.* **2004**, *25*, 1157–1174.

(39) Wang, J.; Wang, W.; Kollman, P. A.; Case, D. A. Automatic Atom Type and Bond Type Perception in Molecular Mechanical Calculations. *J. Mol. Graph. Model.* **2006**, *25*, 247–260.

(40) Dewar, M. J. S.; Zoebisch, E. G.; Healy, E. F.; Stewart, J. J. P. Development and Use of Quantum Mechanical Molecular Models. 76. AM1: A New General Purpose Quantum Mechanical Molecular Model. *J. Am. Chem. Soc.* **1985**, *107*, 3902–3909.

(41) Grest, G. S.; Kremer, K. Molecular Dynamics Simulation for Polymers in the Presence of a Heat Bath. *Phys. Rev. A* **1986**, *33*, 3628–3631.

(42) MacQueen, J. Some Methods for Classification and Analysis of Multivariate Observations. In *Proceedings of the fifth Berkeley symposium on mathematical statistics and probability*; 1967.

(43) Hestenes, M. R.; Stiefel, E. Methods of Conjugate Gradients for Solving Linear Systems. *J. Res. Natl. Bur. Stand. (1934).* **1952**, *49*, 409.

(44) Byrd, R. H.; Lu, P.; Nocedal, J.; Zhu, C. A Limited Memory Algorithm for Bound Constrained Optimization. *SIAM J. Sci. Comput.* **1995**, *16*, 1190–1208.

(45) Field, M. J.; Albe, M.; Bret, C.; Proust-De Martin, F.; Thomas, A. The Dynamo Library for Molecular Simulations Using Hybrid Quantum Mechanical and Molecular Mechanical Potentials. *J. Comput. Chem.* **2000**, *21*, 1088–1100.

(46) Lee, C.; Yang, W.; Parr, R. G. Development of the Colle-Salvetti Correlation-Energy Formula into a Functional of the Electron Density. *Phys. Rev. B* **1988**, *37*, 785–789.

(47) Becke, A. D. Density functional Thermochemistry. III. The Role of Exact Exchange. *J. Chem. Phys.* **1993**, *98*, 5648–5652.

(48) Frisch, M. J.; Trucks, G. W.; Schlegel, H. B.; Scuseria, G. E.; Robb, M. A.; Cheeseman, J. R.; Scalmani, G.; Barone, V.; Petersson, G. A.; Nakatsuji, H.; et al. Gaussian 09, Revision

E.01. Gaussian, Inc.: Wallingford, CT 2009.

(49) Field, M. J.; Bash, P. A.; Karplus, M. A Combined Quantum Mechanical and Molecular Mechanical Potential for Molecular Dynamics Simulations. *J. Comput. Chem.* **1990**, *11*, 700–733.

(50) Jorgensen, W. L.; Maxwell, D. S.; Tirado-Rives, J. Development and Testing of the OPLS All-Atom Force Field on Conformational Energetics and Properties of Organic Liquids. *J. Am. Chem. Soc.* **1996**, *118*, 11225–11236.

(51) Cieplak, P.; Caldwell, J.; Kollman, P. Molecular Mechanical Models for Organic and Biological Systems Going beyond the Atom Centered Two Body Additive Approximation: Aqueous Solution Free Energies of Methanol and N-Methyl Acetamide, Nucleic Acid Base, and Amide Hydrogen Bonding and Chloroform/. *J. Comput. Chem.* **2001**, *22*, 1048–1057.

(52) Baker, J. An Algorithm for the Location of Transition States. *J. Comput. Chem.* **1986**, *7*, 385–395.

(53) Bash, P. A.; Field, M. J.; Karplus, M. Free Energy Perturbation Method for Chemical Reactions in the Condensed Phase: A Dynamic Approach Based on a Combined Quantum and Molecular Mechanics Potential. *J. Am. Chem. Soc.* **1987**, *109*, 8092–8094.

(54) Świderek, K.; Tuñón, I.; Martí, S.; Moliner, V.; Bertrán, J. Role of Solvent on Nonenzymatic Peptide Bond Formation Mechanisms and Kinetic Isotope Effects. *J. Am. Chem. Soc.* **2013**, *135*, 8708–8719.

(55) Marenich, A. V; Cramer, C. J.; Truhlar, D. G. Universal Solvation Model Based on Solute

Electron Density and on a Continuum Model of the Solvent Defined by the Bulk Dielectric Constant and Atomic Surface Tensions. *J. Phys. Chem. B* **2009**, *113*, 6378–6396.

(56) Grimme, S.; Antony, J.; Ehrlich, S.; Krieg, H. A Consistent and Accurate Ab Initio Parametrization of Density Functional Dispersion Correction (DFT-D) for the 94 Elements H-Pu. *J. Chem. Phys.* **2010**, *132*, 154104.

(57) Grimme, S.; Ehrlich, S.; Goerigk, L. Effect of the Damping Function in Dispersion Corrected Density Functional Theory. *J. Comput. Chem.* **2011**, *32*, 1456–1465.

(58) Chipot, C. Free Energy Calculations in Biological Systems. How Useful Are They in Practice; 2006.

(59) Świderek, K.; Paneth, P. Binding Ligands and Cofactor to L-Lactate Dehydrogenase from Human Skeletal and Heart Muscles. *J. Phys. Chem. B* **2011**, *115*, 6366–6376.

(60) Świderek, K.; Martí, S.; Moliner, V. Theoretical Studies of HIV-1 Reverse Transcriptase Inhibition. *Phys. Chem. Chem. Phys.* **2012**, *14*, 12614–12624.

(61) Krzemińska, A.; Paneth, P.; Moliner, V.; Świderek, K. Binding Isotope Effects as a Tool for Distinguishing Hydrophobic and Hydrophilic Binding Sites of HIV-1 RT. *J. Phys. Chem. B* **2015**, *119*, 917–927.

(62) Truhlar, D. G.; Garrett, B. C.; Klippenstein, S. J. Current Status of Transition-State Theory. *J. Phys. Chem.* **1996**, *100*, 12771–12800.

(63) Martí, S.; Moliner, V.; Tuñón, I.; Williams, I. H. QM / MM Calculations of Kinetic Isotope Effects in the Chorismate Mutase Active Site. *Org. Biomol. Chem.* **2003**, *1*,

483–487.

(64) Martí, S.; Moliner, V.; Tuñón, I. Improving the QM/MM Description of Chemical Processes: A Dual Level Strategy to Explore the Potential Energy Surface in Very Large Systems. *J. Chem. Theory Comput.* **2005**, *1*, 1008–1016.

(65) Galmés, M. A.; García-Junceda, E.; Świderek, K.; Moliner, V. Exploring the Origin of Amidase Substrate Promiscuity in CALB by a Computational Approach. *ACS Catal.* **2019**.

(66) Abdulmalek, E.; Arumugam, M.; Mizan, H. N.; Abdul Rahman, M. B.; Basri, M.; Salleh, A. B. Chemoenzymatic Epoxidation of Alkenes and Reusability Study of the Phenylacetic Acid. *Sci. World J.* **2014**, *2014, Article ID 756418*.

(67) Liu, W.; Chen, J.; Liu, R.; Bi, Y. Revisiting the Enzymatic Epoxidation of Vegetable Oils by Perfatty Acid: Perbutyric Acid Effect on the Oil with Low Acid Value. *J. Am. Oil Chem. Soc.* **2016**, *93*, 1479–1486.

(68) Chen, J.; Zhou, J.; Liu, W.; Bi, Y.; Peng, D. Enzymatic Epoxidation of Soybean Oil in the Presence of Perbutyric Acid. *Chem. Pap.* **2017**, *71*, 2139–2144.